# Eruptive versus confined X-class flares in solar cycles 23 and 24

Rositsa Miteva
Institute of Astronomy and National Astronomical Observatory, Bulgarian Academy of Sciences, BG-1784, Sofia
rmiteva@astro.bas.bg
(Submitted on 16.01.2021; Accepted on 04.03.2021)

**Abstract.** A systematic analysis on the properties of all GOES X-class solar flares (SFs) in solar cycles 23 and 24 (1996−2019) is performed. The occurrence rates and parameters of the eruptive and confined SFs are presented. The aspect of eruptivity versus confinement is investigated with respect to the co-occurrence of coronal mass ejections (CMEs), radio emissions, energetic protons and geomagnetic storms. The absence of interplanetary type III radio bursts, in addition to the lack of CMEs, is found to be a very good proxy for confinement, in contrast to the sunspot type of the parent active region, as both eruptive and confined SFs are predominantly of $\beta$-$\gamma$-$\delta$ magnetic type. The remaining parameters, protons and geomagnetic storms, imply observing from a specific location in the heliophere and thus are biased for Earth-reaching phenomena. Finally, the relationships between the two types of SFs and the considered here solar activity phenomena are discussed in view of previous studies.
**Key words:** solar flares (SFs) - coronal mass ejections (CMEs) - interplanetary type III radio bursts (IP III) - solar energetic particles (SEPs) - geomagnetic storms (GSs)

## 1 Introduction

One of the major examples of solar eruptive activity is a solar flare (SF), a short-lived and very energetic event in the solar atmosphere, e.g., Fletcher et al. (2011). This is a complex phenomenon occurring usually in the vicinity of active regions (ARs) and constitutes a release of the stored magnetic energy via a process known as magnetic reconnection (e.g., Shibata and Magara, 2011). Commonly, SFs are regarded as the flash (i.e., the electromagnetic (EM) emission) observed on solar images (Benz, 2016), usually in extreme ultraviolet (EUVs), soft X-rays (SXRs), hard X-rays (HXRs) and radio wavelengths, though rarely in white light, as in the famous space weather case of 1st September 1859, the so-called Carrington-Hodgson event (Carrington, 1859 and Hodgson, 1859). Apart from the EM emission, SFs are accompanied with mass motion, acceleration of particles, magnetic field line reconfiguration. The latter is attested by the close relationship between SFs and coronal mass ejections (CMEs), large ammount magnetized plasma expelled from the solar corona into the interplanetary (IP) space and regarded as another outcome of a solar eruption (e.g., Webb and Howard, 2012). Namely, the largest (in SXRs) SFs have been shown to be always accompanied by CMEs (Harrison, 1995, Yashiro et al. 2005) supporting earlier results on the link between long-duration SFs and CMEs (Kahler et al. 1989).

Most often in the literature eruptive SFs are those associated with CMEs, whereas the confined ones lack large scale eruptions, as proposed early on by Svetska (1986) and adopted in follow up studies. For example, Wang and Zhang (2008) investigated the X-class flares from 1996 to 2004 and based on these 104 cases found 90-to-10% prevalence of the eruptive SFs. Furthermore they indicated that eruptive SFs are closer to the flux-weighted magnetic center of

the ARs and that there is stronger overlying arcade field over the confined flares, supported later also by, e.g., Cheng et al. (2011) and Baumgartner et al. (2018). Cheng et al. (2011) investigated nine M- and X-class flares from the same AR and found out that eruptive flares have longer duration, extended EUV brightenings, are located in the outskirts of the AR and the overlying transverse magnetic field is weaker. 44 SFs in solar cycle (SC) 24 were investigated by Baumgartner et al. (2018) in terms of flare offset from the AR center, regarded as compact or extended. Other promising parameters listed there are the strength and orientation of the coronal magnetic field, and polarity inversion line (PIL) orientation. The properties of 18 confined flares in 2011−2017 were examined by Li et al. (2019) in terms of differentiating in magnetic topologies and acceleration scenarios. Furthermore Tschernitz et al. (2018) inspected 32 confined and 19 eruptive SF from B to X-class with respect to their ribbon areas and the fraction of the magnetic flux that take part in the reconnection process. Based on their analysis, they also provided an estimate for an upper limit of SF, that exceeds the observations by more than an order of magnitude. In summary, the majority of these and other studies focus on the properties of the magnetic fields in the surroundings of the AR in terms of flux ratio between low and high altitude magnetic fields, decay index, magnitude of transverse magnetic field or its orientation with respect to the PIL, magnetic helicity, see, e.g., Nindos and Andrews (2004), Zucarello et al. (2017), Li et al. (2019) and the references therein.

Investigation of the magnetic configuration of the AR producing the X-class SFs goes beyond the present analysis, as an alternative approach is adopted here. Namely, the aspect of eruptivity is regarded as the ability of plasma, electromagnetic emission and/or particles to escape from the Sun or, alternatively, magnetic fields to adopt an 'open' configuration, implying some restructuring taking place in the solar atmosphere. The latter aspect was recognized early on by Green et al. (2002) as requisite for eruptive flares. As a direct evidence for the established connection between the corona and IP space is regarded the CME propagation. Another, indirect evidence is also well known, namely radio emission from so-called type III bursts (e.g., Pick and Vilmer, 2008), as these are the radio signatures of electron beams traveling along open magnetic field lines. Both, CME and type III observations are done via remote sensing technique, namely without imposing spatial requirement between the observer and the events to be fulfilled in order to enable their detection. In the case of in situ observations, the number of the specific solar/IP phenomena is limited to those arriving at the location of the instrument (a satellite in space, or ground-based observatory). For example, the direct observations of solar energetic particles (SEPs, e.g., Desai and Giacalone, 2016, Klein and Dalla, 2017) require space-borne instruments capable to detect protons, electrons and/or heavy ions in various energies and coming along established magnetic pathway. Similarly, when detecting geomagnetic storms (GSs, e.g., Lakhina and Tsurutani, 2016), the series of equatorially situated magnetometers detect the drop in the terrestrial magnetic field due to the magnetic structure impinging on the magnetosphere. In the latter two cases, the records do not exclude the (co-)existence of other SEPs and GSs in the heliosphere. Thus, only a lower number of all possible SEP and GS events is possible while observing them from a single point in space (e.g., Earth). The space weather relevance of all

these eruptive events is well-known and a subject of ongoing analysis for their successful now- and/or forecasting (Pulkkinen, 2007).

For the purpose of this work 'eruptivity' is defined as the association between a given SF and another solar activity phenomenon, namely CMEs close to the Sun and/or type III radio bursts in the IP space, and to a lesser extent also SEPs or GSs. Alternatively, a 'confinement' is defined as the lack of co-occurrence of any of the considered above solar events with respect to the SF.

In the present study, the eruptivity versus confinement identity of the largest (X-class) SFs is investigated. The considered time period is 1996−2019, covering SCs 23 and 24, also due to the improved availability of remote sensing data in the last two SCs.

## 2 Data analysis and association procedure

For the purpose of developing novel methods for the identification of eruptive versus confined SF events, the following solar and space weather phenomena are selected: SFs, CMEs, IP IIIs, SEPs, GSs and magnetic configurations of the SF-related AR (or sunspot group). Each data source, analysis and inter-association procedures are described below.

### 2.1 Solar flares (SFs)

All SFs of X-class (defined as peak SXR flux in the GOES 1−8 Å channel of $\geq 10^{-4}$ W m$^{-2}$) are initially selected in the considered time period, 1996−2019. Ready SF catalogs are used[1] for this purpose. We adopt as reported there: date, X-class, onset, peak and end times, location (in helio-longitudes and latitudes) and AR number. The first X-class flare took place in 1996, whereas the last one occurred in 2017, leading to 175 cases in total. This constitutes the initial event list for this study, provided also as online material.

### 2.2 Associated phenomena

CME information is collected from the SOHO/LASCO CDAW catalog[2], still used widely as a standard source of information on the occurrence and properties of CMEs since 1996. SFs and CMEs are considered to be two representatives of the same solar activity when they occur in a close succession (e.g., the reported time of first appearance of the CME above the occulting disk of the SOHO/LASCO instrument is after the SF onset, but within 1−2 hour of the SF peak time) and both originate from the same solar quadrant. The same procedure for association is used in Miteva et al. (2013).

IP type III radio bursts from Wind/WAVES instrument are used by inspecting the available radio dynamic spectra[3] in the frequency range from

[1] ftp://ftp.swpc.noaa.gov/pub/warehouse
[2] https://cdaw.gsfc.nasa.gov/CME$_list$/
[3] https://urap.gsfc.nasa.gov/cgi-bin/waves$_plots.pyandhttps$ : //$cdaw.gsfc.nasa.gov/CME_list/$

nearly 14 MHz down to 20 kHz (e.g., emission that is close to Earth). The association with radio bursts is done according to the time overlap between the reported radio emission occurrence and the flare (or CME) timings. The identification of the IP III timing is done at 1 MHz with 1−2 minute precision.

For completeness, the classification of the SF-associated sunspot or AR magnetic field configuration is provided below[4]:

- $\alpha$: A unipolar sunspot group.
- $\beta$: A sunspot group having both positive and negative magnetic polarities (bipolar), with a simple and distinct division between the polarities.
- $\gamma$: A complex active region in which the positive and negative polarities are so irregularly distributed as to prevent classification as a bipolar group.
- $\beta$-$\gamma$: A sunspot group that is bipolar but which is sufficiently complex that no single, continuous line can be drawn between spots of opposite polarities.
- $\delta$: A qualifier to magnetic classes indicating that umbrae separated by less than 2 degrees within one penumbra have opposite polarity.
- $\beta$-$\delta$: A sunspot group of general beta magnetic classification but containing one (or more) delta spot(s).
- $\beta$-$\gamma$-$\delta$: A sunspot group of beta-gamma magnetic classification but containing one (or more) delta spot(s).
- $\gamma$-$\delta$: A sunspot group of gamma magnetic classification but containing one (or more) delta spot(s).

Solar energetic proton association with their solar origin, SF and CME is a well known problem in the literature, but several consisting procedures have been proposed, see e.g., Cane et al. (2010), Papaioannou et al. (2016), Miteva et al. (2013, 2018). Despite the observer subjectivity, similar results are found (see, however, a discussion in Miteva (2019) on the possible differences). In this study, 17−22 MeV proton data[5] (Miteva et al. 2020) as observed from the SOHO/ERNE instrument (Torsti et al. 1995) is used and the proton amplitudes are measured in differential proton flux units (DPFU)[6].

Finally, identifications of GSs based on the 1-hr disturbance storm index (Dst) index are selected, as reported by the Kyoto database[7], using the procedure presented in Miteva (2020).

## 3 Results

### 3.1 Properties of the SFs

#### 3.1.1 SF class

In Fig. 1, on the left, the yearly histogram of the SF occurrence is presented, covering the time period of SC23 (highlighted with blue color) and 24 (with gray) using 6-month binning. The same color code is used throughout the

[4] https://www.spaceweather.com/glossary/magneticclasses.html
[5] https://catalogs.astro.bas.bg/
[6] 1 DPFU = 1 proton $cm^{-2}$ $s^{-1}$ $sr^{-1}$ $MeV^{-1}$
[7] http://wdc.kugi.kyoto-u.ac.jp/wdc/Sec3.html

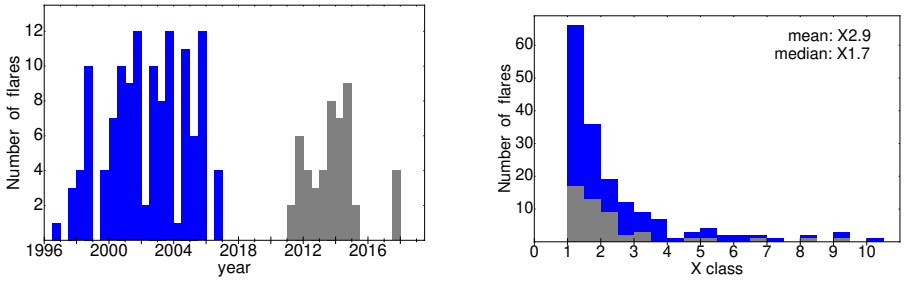


**Fig. 1.** Distributions of the SFs over SC23 (blue) and SC24 (gray) on the left with 6-month time bin, and on the right is plotted the SF class up to X10.

paper. 126 X-class flares are reported in SC23, compared to 61% less in SC24 (49 cases).

The right plot shows the distribution of the SF class by means of a stacked histogram. The number of X-class flares in SC23 is given by the height of the blue bar, whereas those in SC24 are shown in gray. The sum gives the number of events for each bin, chosen to be of size 0.5. The majority of the X-class SFs has values from X1 to X3 (134 cases), and for clarity purposes only up to X10 is shown in the graph, leaving out 5 sparsely distributed flares up to the maximum observed value of X28. The mean (median) value for the entire sample is X2.9 (X1.7). The same median values are obtained for both SCs, whereas larger mean is calculated for SC23 (X3.1) and lower for SC24 (X2.3).

### 3.1.2 SF SXR intensity profile

Apart from the maximum of the SXR intensity of the SF, here the focus is on the timings from the onset to the maximum (referred to as 'rise') and from the maximum to the end ('decline' or decay) time. Figure 2 presents the results. The top row shows the histograms of the rise and decline times binned into 2 minutes. The SF rise has on average (for the entire time period) longer duration, with mean (median) values of 21 minutes (15 minutes), compared to the mean (median) SF decline time of 14 minutes (10 minutes), respectively. Alternatively, the same data is presented as a ratio to the particular SF duration, as shown in the lower row. The rise times take on average 60% of the flare reported duration, whereas the decline is shorter (40%).

### 3.1.3 SF location

Finally, the heliographic location of the SFs over the solar disk is investigated. The left panel of Fig. 3 shows the distribution of the helio-latitude and on the right is given the helio-longitude. The X-class flares are distributed in 30 degree bands around the equator, with slight prevalence to southern hemisphere over the last two SCs (median for the entire period is S07). With respect to the longitude, the distribution is nearly flat, with slight increase in the bin centered at W20 (with median at W11 for the entire sample).

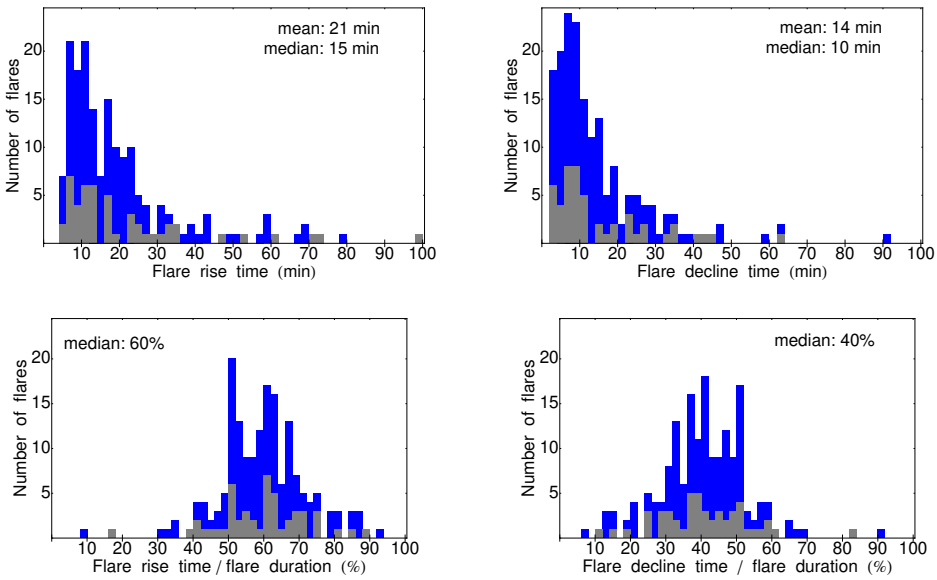


**Fig. 2.** Distributions of SF onset-to-peak or rise (left) and peak-to-end or decline times (right), as absolute duration (top) and as a fraction of total SF duration (bottom).

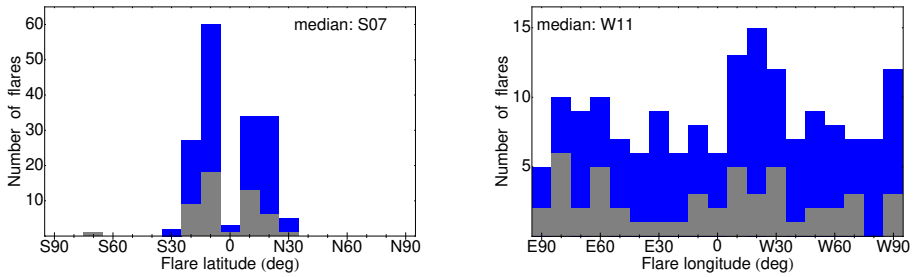


**Fig. 3.** Helio-latitude (left) and longitude (right) for the SFs.

## 3.2 Properties of the SF-associated phenomena

### 3.2.1 CMEs

The X-class associated CMEs are 133 due to multiple data gaps (17), 2 uncertain cases or no clear features at the time of the flare (23). The properties of the so-identified CMEs are shown in Fig. 4, separately for the CME projected speed (the left panel) and angular width, AW (the right panel). The CME distribution has a large span in speeds, from 200 $\mathrm{km\,s^{-1}}$ to the maximum value ever observed 3500 $\mathrm{km\,s^{-1}}$. The mean (median) values for the entire sample is 1285 $\mathrm{km\,s^{-1}}$ (1124 $\mathrm{km\,s^{-1}}$) for the speed and 277 degrees (360 degrees) for the

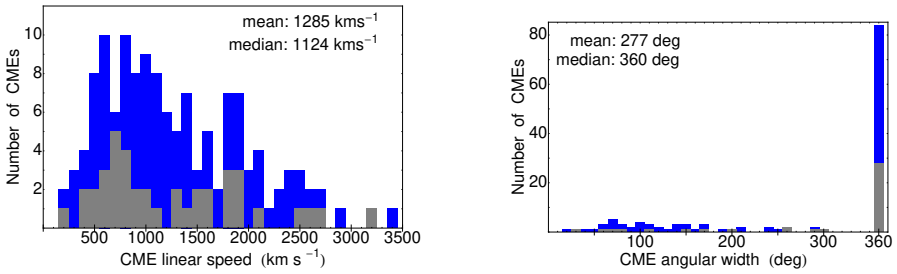


**Fig. 4.** Distributions of the CME projected speed (left) and angular width (right).

AW. The bin width for the plots is 100 km s$^{-1}$ and 10 degrees, respectively. The respective mean values for the speed and AW in SC23 (1302 km s$^{-1}$ and 266 degrees) are closer to those for the entire sample (1285 km s$^{-1}$ and 277 degrees), compared to those in SC24 (1244 km s$^{-1}$ and 301 degrees). The median values of AW are the same for all three time periods, namely there is a prevalence of halo CMEs. Slightly larger median values for the CME speed are obtained in SC23 (1150 km s$^{-1}$) and the entire period (1124 km s$^{-1}$), compared to the value in SC24 (996 km s$^{-1}$).

For completeness, the Pearson correlation coefficients between the $\log_{10}$ of the SF class and CME speed or AW have been calculated, obtaining rather low values, $0.39 \pm 0.06$ and $0.23 \pm 0.06$, respectively, based on 133 pairs in either case. The uncertainty is provided using the bootstrapping method, based on 1000 calculations (see, e.g., Miteva et al. 2013).

### 3.2.2 IP type III radio bursts

Radio data from Wind/WAVES was found for 169 out of all 175 cases. IP type III bursts are identified in 131 cases (78%) and prominent radio features lacked in 38 of the cases (22%). 77 (59%) of the type IIIs started during the rise phase of the SF, whereas 54 (41%) occurred close to the peak (±2 min) or during the decline phase. Note that the radio intensity is not taken into account, only the occurrence of the features. Furthermore, the radio emission in the low and middle corona is not considered for the purpose of this work. As evidence for the escape into IP space only Wind/WAVES type IIIs are recognized.

### 3.2.3 Sunspot magnetic configuration

With respect to the underlying magnetic field configuration of the AR, the obtained results are given in Table 1. The number of cases in the respective sunspot magnetic field configurations (six combinations in total denoted with Greek letters) are given. For the entire sample, second column, there are 132 identifications. No additional restrictions are imposed in this case. The largest subsample is the one of the most complex AR ($\beta$-$\gamma$-$\delta$), 75/132 (57%). Two

**Table 1.** Number of events with the denoted magnetic configuration of the SF-associated AR.

| Sunspot types or misc. | Entire sample | CMEs yes | CMEs no | IP IIIs yes | IP IIIs no | CMEs and IP IIIs both | CMEs and IP IIIs neither |
|---|---|---|---|---|---|---|---|
| $\alpha$ | 3 | 2 | 1 | 1 | 2 | 1 | 1 |
| $\beta$ | 24 | 18 | 1 | 21 | 3 | 16 | 1 |
| $\beta$-$\gamma$ | 20 | 16 | 2 | 15 | 4 | 14 | 2 |
| $\beta$-$\delta$ | 9 | 7 | 1 | 7 | 2 | 6 | 1 |
| $\gamma$-$\delta$ | 1 | 1 | – | 1 | – | 1 | – |
| $\beta$-$\gamma$-$\delta$ | 75 | 60 | 13 | 52 | 19 | 52 | 13 |
| all types | 132 | 104 | 18 | 97 | 30 | 90 | 18 |
| uncertain | 3 | 3 | – | 3 | – | 3 | – |
| not reported | 40 | 26 | 5 | 31 | 8 | 25 | 5 |
| all events | 175 | 133 | 23 | 131 | 38 | 118 | 23 |

other types have nearly the same event numbers, 24 $\beta$ (18%) and 20 $\beta$-$\gamma$ (15%) configurations, whereas $\beta$-$\delta$ type has only nine cases (7%). The sum of all types in the column is given in the row denoted with 'all types'. The final event number in a specific category denoted by 'all events' is the sum of the previous three entries, including all uncertain cases, lack of observation reports and 'all types'.

These fractions are kept even if some specific additional requirements are made. Namely, the presence or not of CME, IP type III or when both/neither phenomena occurred in addition to the identified AR type. The results are summarized in the remaining six columns in Table 1. Namely, when the occurrence of a CME is demanded, the largest percentage is again for the $\beta$-$\gamma$-$\delta$, 58% (60/104), whereas 17% (18/104) goes for $\beta$-type configuration and 15% (16/104) for $\beta$-$\gamma$. Under the requirement of IP III occurrence, the percentages for the same sunspot types are 54% (52/97), 22% (21/97) and 15% (15/97), respectively. Similar fractions to the above two sets of results are obtained when it is insisted on the co-occurrence of both CMEs and IP type IIIs (see penultimate column in Table 1).

The opposite requirement, namely the lack of CME and IP III features is fulfilled for a lower number of events: neither phenomena could be identified for 18 cases, among which, the majority, 13, have $\beta$-$\gamma$-$\delta$ configuration, and two cases are $\beta$-$\gamma$. Note that under the sole condition for the absence of IP IIIs, we obtain 30 cases, again the majority 63% (19/30) originate from $\beta$-$\gamma$-$\delta$ sunspot configuration, whereas the remaining types have just a few cases each.

### 3.2.4 Protons and geomagnetic storms

With respect to in situ observed proton events, there are 66 cases identified in the 17−22 MeV energy channel of the SOHO/ERNE instrument. The distribution of the peak intensity of the differential proton flux of the sample is shown in the left panel of Fig. 5. The mean value of the proton peak intensity is 1.05 DPFU whereas the median is 1.34 DPFU, for the entire particle sample.

There are only 20 GSs associated to have origin at the SF-associated CMEs. Despite the low event number, the distribution in terms of Dst index is presented in Fig. 5 (right), where the majority are in fact minor storms, with Dst index between −100 and −150 nT.

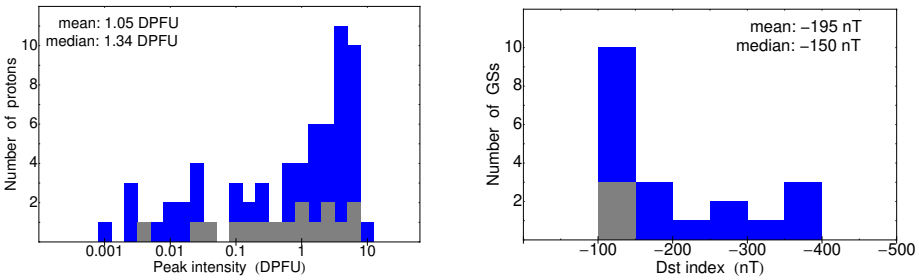


**Fig. 5.** Distribution of peak values of differential proton flux (left) and geomagnetic storm Dst index (right).

### 3.3 Eruptivity versus confinement

With respect to the SFs, there are four other types of solar activities that may be considered as a criterion for eruptivity of a SF: apart from the occurrence of CME, other phenomena such as IP type III, SEP and/or GS could be co-present. The strict definition for eruptive flares would require all accompanied 4 types to be present, whereas the strict requirement for confined would be none of them to co-occur. In the general case, eruptive SFs are those associated with CMEs or/and IP type IIIs, or in some other combination of the solar events from the above list. The results are summarized in Table 2.

Table 2 lists the event type (SF, CME, IP III, p, GS), occurrence rate, mean and median values of the considered event type. The occurrences are calculated as a fraction of occurrence to all observed cases after excluding the data gaps (namely the latter is the sum of all actual occurrences and identified absences).

Eruptive SFs resulted into four categories, depending on the requirement applied, from all phenomena to be co-present down to the occurrence of CMEs only. Alternatively, confined flares should lack any other solar activity feature. SF class is larger for the eruptive flares (in any of the sub-category), both in mean and median values compared to the confined SFs. Flare rise and decline times are also longer for eruptive compared to confined SFs by nearly half of the value.

Comparing between several definitions for eruptive flares, one can easily notice that in the strict case (top) the mean and median CME speed are the largest, lowering by about $100-200$ km s$^{-1}$ in the remaining ones. A decrease is also obtained in the proton amplitude (compare the respective values in the top two eruptive SF categories).

The occurrence of the remaining parameters, in situ observed protons and GSs, imply that they have been observed at Earth. Thus, one may expect that the obtained results are only a lower limit of all Earth-facing phenomena, as many may miss the Earth. This fact imposes an intrinsic observational limitation for these two parameters.

**Table 2.** Summary of the properties of SFs and their accompanied phenomena. Occurrence rate is given in percentage (and as a fraction between the observed events and the event sample). Mean and median values are calculated for: SF class/rise time/decline time (in minutes); CME projected speed (in $\mathrm{km\,s^{-1}}$)/AW (in degrees); proton ('p') amplitude (in DPFU); Dst index of the GS (in nT).

| Eruptive/Confined (accompanied events) | Event type | Occurrence rate | Mean value | Median value |
|---|---|---|---|---|
| **Eruptive** | | | | |
| (CME-IP III-p-GS) | SF | 7% (13/175) | X5.6/29/17 | X3.4/18/14 |
| | CME | 8% (13/158) | 1526/345 | 1571/360 |
| | IP III | 8% (13/169) | – | – |
| | p | 8% (13/169) | 3.42 | 2.93 |
| | GS | 7% (13/175) | −217 | −162 |
| **Eruptive** | | | | |
| (CME-IP III-p) | SF | 35% (61/175) | X3.8/25/16 | X2.0/17/12 |
| | CME | 39% (61/158) | 1426/310 | 1250/360 |
| | IP III | 36% (61/169) | – | – |
| | p | 35% (61/175) | 2.1 | 1.34 |
| **Eruptive** | | | | |
| (CME-IP III) | SF | 67% (118/175) | X3.0/23/16 | X1.8/17/12 |
| | CME | 75% (118/158) | 1332/293 | 1218/360 |
| | IP III | 70% (118/169) | – | – |
| **Eruptive** | | | | |
| (CME) | SF | 84% (133/158) | X2.9/23/15 | X1.8/17/11 |
| | CME | 84% (133/158) | 1285/277 | 1124/360 |
| **Confined** | | | | |
| (none) | SF | 13% (23/175) | X1.5/14/12 | X1.2/9/6 |

## 4 Discussion and Conclusion

There are 23 events defined as confined SFs in this study, as neither CMEs nor other solar phenomena (radio emission, energetic particles or GSs) are detected. The majority of these cases are already reported in several earlier works: multiple evens from SC23 in Wang and Zhang (2007), single cases can be found, e.g., in Cheng et al. (2011), Baumgartner et al. (2018), Tschernitz et al. (2018), Li et al. (2019) as selected cases in SC23 or SC24. Three newly confined flares are proposed here. Overall for the entire sample of X-class flares, 13% are identified as confined SFs over a period of both SCs, 12% is in SC23 and 17% in SC24, consistent with the 10% result obtained by Wang and Zhang (2007) for SC23.

Furthermore, a comprehensive summary on the occurrence rate and properties of eruptive and confined SFs over two SCs is presented here, as well as their accompanied solar phenomena, if any. The definition for eruptivity versus confinement is primarily based on the association or not of CMEs, as well known by previous studies. In addition, here the co-association of radio emission signatures of escaping electrons is explored together with the presence of in situ protons or geomagnetic storms at Earth.

It was found that the condition of absence of IP type III radio bursts is a very good proxy for confinement, as all SF lacking CMEs also lack IP type IIIs. The opposite conditions is also true in general terms, with over 90% success rate.

The underlying sunspot (or AR) magnetic configuration does not seem to be an ordering parameter, as in either SF category the majority of the events are of $\beta$-$\gamma$-$\delta$ type. As stated in numerous previous studies, the overlying magnetic field strength, its structure and dynamic is decisive for the eruptive properties of the X-class productive AR. The (large) M-class flares are a natural expansion of this work and a study of their eruptive properties will be presented elsewhere.

## Acknowledgement

The author acknowledges the provided support by the Bulgarian National Science Fund with contract No. KP-06-H28/4 (08-Dec-2018). Results from this work are included in the inter-academy collaboration project between Bulgaria and Serbia: Active events on the Sun; Catalogs of proton events and electron signatures in X-ray, EUV and radio diapason; Influence of collisions on optical properties of dense hydrogen plasma (2020). The use of SOHO/ERNE data, solar flare and CME catalogs is greatly appreciated. The author thanks the radio monitoring service at LESIA (Observatoire de Paris) that provides value-added data that have been used for this study, especially data from Wind/WAVES. The CME catalog is generated and maintained at the CDAW Data Center by NASA and The Catholic University of America in cooperation with the Naval Research Laboratory. SOHO is a project of international collaboration between ESA and NASA.

## References

Baumgartner, Ch., Thalmann, J. K., Veronig, A. M., 2018, *The Astrophysical Journal*, **853: 2**, article id. 105, 11 pp.
Benz, A. O., 2016, *Living Reviews in Solar Physics*, **14**, Article number: 2, 59 pp.
Cane, H. V., Richardson, I. G., von Rosenvinge, T. T., 2010, *Journal of Geophysical Research*, **115: A8**, CiteID A08101
Carrington, R. C., 1859, *Monthly Notices of the Royal Astronomical Society*, **20**, pp. 13–15
Cheng, X., Zhang, J., Ding, M. D., Guo, Y., Su, J. T., 2011, *The Astrophysical Journal*, **732: 87**, 8 pp.
Desai, M., Giacalone, J., 2016, *Living Reviews in Solar Physics*, **13: 1**, article id. 3, 132 pp.
Fletcher, L., Dennis, B. R., Hudson, H. S., Krucker, S., Phillips, K., Veronig, A., Battaglia, M., Bone, L., Caspi, A., Chen, Q., Gallagher, P., Grigis, P. T., Ji, H., Liu, W., Milligan, R. O., Temmer, M., 2011, *Space Science Reviews*, **159: 1-4**, pp. 19–106
Green, L. M., Matthews, S. A., van Driel-Gesztelyi, L., Harra, L. K., Culhane, J. L., 2002, *Solar Physics*, **205**, pp. 325–339
Harrison, R. A., 1995, *Astronomy and Astrophysics*, **304**, pp. 585–593
Hodgson, R., 1859, *Monthly Notices of the Royal Astronomical Society*, **20**, pp. 15–16
Kahler, S. W., Sheeley, N. R., Jr., Liggett, M., 1989, *The Astrophysical Journal*, **344**, pp. 1026–1033
Klein, K.-L., Dalla, S., 2017, *Space Sci. Rev.*, **212**, pp. 1107–1136
Lakhina, G. S., Tsurutani, B. T., 2016, *Geoscience Letters*, **3**, article id.5, 11 pp.
Li, T., Liu, L., Hou, Y., Zhang, J., 2019, *The Astrophysical Journal*, **881: 151**, 20 pp.
Miteva, R., Klein, K.-L., Malandraki, O., Dorrian, G., 2013, *Solar Physics*, **282**, pp. 579–613
Miteva, R., Samwel, S. W., Costa-Duarte, M. V., 2018, *Solar Physics*, **293**, id. 27, 44 pp.
Miteva, R., 2019, *Bulgarian Astronomical Journal*, **31**, pp. 55–67
Miteva, R., Samwel, S. W., Zabunov, S., 2020, *Bulgarian Astronomical Journal*, **33**, pp. 99–108
Miteva, R., 2020, *Advances in Space Research*, **66:8**, pp. 1977–1991
Nindos, A., Andrews, M. D., 2004, *The Astrophysical Journal*, **616**, pp. L175–L178

Papaioannou, A., Sandberg, I., Anastasiadis, A., Kouloumvakos, A., Georgoulis, M. K., Tziotziou, K., Tsiropoula, G,. Jiggens, P., Hilgers, A., 2016, *Journal of Space Weather and Space Climate*, **6**, id.A42, 29 pp.
Pick, M., Vilmer, N., 2008, *The Astronomy and Astrophysics Review*, **16**, pp. 1–153
Pulkkinen, T., 2007, *Living Reviews in Solar Physics*, **4: 1**, article id. 1, 60 pp.
Shibata, K., Magara, T., 2011, *Living Reviews in Solar Physics*, **8**, article id. 6, 99 pp.
Svestka, Z., 1986, *in The lower atmosphere of solar flares; Proceedings of the Solar Maximum Mission Symposium, Sunspot, NM, Aug. 20-24, 1985 (A87-26201 10-92), Sunspot, NM, National Solar Observatory*, pp. 332–355
Torsti, J., Valtonen, E., Lumme, M., Peltonen, P., Eronen, T., Louhola, M., Riihonen, E., Schultz, G., Teittinen, M., Ahola, K., Holmlund, C., Kelhä, V., Leppälä, K., Ruuska, P., Strömmer, E., 1995, *Solar Physics*, **162**, pp. 505–531
Tschernitz, J., Veronig A. M., Thalmann, J. K., Hinterreiter, J., Pötzi, W., 2018, *The Astrophysical Journal*, **853:41**, 16 pp.
Wang, Y., Zhang, J., 2007, *The Astrophysical Journal*, **665: 2**, pp. 1428–1438
Webb, D. F., Howard, T. A., 2012, *Living Reviews in Solar Physics*, **9: 1**, article id. 3, 83 pp.
Yashiro, S., Gopalswamy, N., Akiyama, S., Michalek, G., Howard, R. A., 2005, *JGRA*, **110: A12**, A12S05, 11 pp.
Zucarello, F. P., Chandra, R., Schmieder, B., Aulanier, G., Joshi, R., 2017, *Astronomy and Astrophysics*, **601**, A26, 11 pp.